Revision 2

XANES Measurements of Cr Valence in Olivine and Their Applications to Planetary Basalts

A.S. Bell[1]*, P.V. Burger[1], Loan Le[2], C.K. Shearer[1], J.J. Papike[1], S.R. Sutton[3], M. Newville[3], and J. Jones[2]

[1]Institute of Meteoritics, Department of Earth and Planetary Sciences, University of New Mexico, Albuquerque New Mexico 87131 [2]ESCG, Houston, TX 77058[3]KR, NASA/ JSC, Houston, TX 77058
[3]Center for Advanced Radiation Sources, University of Chicago, Chicago IL, 60637

Abstract

In this work we present a series of experiments that examine the relationship between oxygen fugacity and Cr valence ratio in olivine grown from a basaltic liquid. These experiments are specifically targeted for an olivine-rich martian basalt composition that was modeled after the bulk chemistry of the meteorite Yamato 980459 (i.e., Y-98). The chromium valence ratio in the olivine crystals was measured with X-ray-Absorption-Near-Edge-Spectroscopy (XANES) at the Advanced Photon Source, Argonne National Laboratory. Results from the XANES measurements indicate that the ratio of divalent to trivalent Cr in the olivine is not only systematically correlated with fO_2, but is also reflective of the molar Cr^{3+}/Cr^{2+} in the silicate liquid from which it grew. In this way, measurements of Cr valence in olivine phenocrysts can yield important information about the oxygen fugacity and molar Cr^{3+}/Cr^{2+} of its parental liquid in the absence of a quenched melt phase. Although the results from the experiments presented in this work specifically apply to the Y-98 parental melt, the concepts and XANES analytical techniques discussed within the text present a novel, generalized methodology that may be applicable to any olivine-bearing basalt. Furthermore, the XANES-based measurements are made on a micron-scale, thus potential changes of the Cr^{3+}/Cr^{2+} in the melt during crystallization could be examined with a great deal of spatial detail.

Introduction

Oxidation state, basaltic magmas, and their mantle sources

Quantifying and understanding the redox evolution of basaltic liquids and their mantle source regions has been a major theme in magmatic petrology for over thirty years (Fuldali 1965; Arculus et al. 1981; Ballhaus 1993; Carmichael 1991; Brandon and Draper 1996; Canil 2002; Kelly and Cottrell 2009). Oxygen fugacity is a critical variable that exerts profound influence on basaltic phase equilibria, magmatic differentiation paths, C-O-H-S volatile speciation, metallic core segregation, and even peridotite rheology (Mathez 1984; Wood et al. 1990; Carmichael 1991; Righter 2003; Shearer et al. 2006; Mackwell 2008). In general, calculating the oxidation state of planetary basalts is a rather vexing problem. Oxygen fugacity calculations for planetary basalts are frequently impeded by: (1) the paucity of glassy material that could be used to infer fO_2 from direct measurements of Fe^{2+}/Fe^{3+}; (2) difficulties associated with redox-sensitive mineral assemblages that are susceptible to subsolidus re-equilibration (e.g. the Fe-Ti oxides); and (3) understanding how calculated fO_2 values fit into the temporal evolution and petrologic context of the sample. More often than not, the relationship between the fO_2 values calculated for a crystallized basaltic sample and the fO_2 of its mantle source region is difficult to discern due to post-melting compositional modification during ascent and differentiation.

Despite these difficulties, many studies have produced robust fO_2 estimates for the olivine-phyric SNC (Shergottite-Nakhlite-Chassignite) suite meteorites. These estimates have been made using a variety of different oxybarometers. The fO_2 values calculated for the olivine-phyric martian basalts show a curious degree of dispersion in that the calculated fO_2 values range from IW-0.5 to IW+4.4 (Wadhwa 2001; Herd et al. 2003; and Shearer et al. 2006). Calculated fO_2

values have even been observed to vary by two to three orders of magnitude in a single sample depending on which mineral pairs and compositions were used in the calculations.

In light of these difficulties and uncertainties, there is naturally much impetus to develop more sensitive methods with which to calculate fO_2 values for not only the olivine-phyric martian meteorites, but also a generalized methodology that is applicable to any crystallized basaltic material. Measurements of the formal valence state of trace Cr that is present in olivine present a potential solution to this problem. Such measurements may yield important insight into the oxidation state of the parental liquid while circumventing problems associated with the lack of glassy material or reset mineral equilibria.

The utility of chromium as a petrogenetic tracer and a redox indicator

The consequences of variable Cr^{3+}/Cr^{2+} in basaltic melts have long been recognized as playing a critical role in dictating the geochemical behavior and distribution of Cr in mantle-derived basalts (Irving 1975; Delano 1990; Papike et al. 2005; and Karner et al. 2007). Understanding the interplay between Cr valence and fO_2 in primitive basaltic magmas is a prerequisite for developing petrogenetic models of lunar, terrestrial and planetary basalts, as well as constraining the composition of their mantle sources. The study of Schreiber and Haskin (1976) suggested that measurements of Cr valence in experimentally-produced melts would help illuminate the link between Cr geochemistry and its valence ratio in lunar and planetary basalts. However, a comprehensive understanding of Cr redox systematics in silicate liquids has been hindered by the difficulty of interpreting Cr valence measurements. For example, quench-induced modification of the Cr^{2+}/Cr^{3+} ratio in ferric iron-bearing silicate liquids muddied the understanding of Cr redox equilibria in silicate liquids (Schrieber and Haskin 1976). Recent pioneering efforts of Berry and O'Neill (2004, 2006) have begun to illuminate the behavior of Cr

in Fe-free systems, but the direct measurement of Cr valence in natural Fe-bearing glasses remains a difficult analytical problem because the fO_2 range over which Cr^{2+} is oxidized to Cr^{3+} overlaps that of the homogenous ferric-ferrous equilibria for many basaltic liquid compositions.

Cr valence in olivine as a proxy for the liquid

Proxy measurements of Cr valence in near-liquidus phases present a natural solution to this problem. Olivine is a prime candidate for three reasons: 1) Olivine is the liquidus phase in many basalts of planetary origin; 2) Olivine does not show strong preference for one valence state of Cr over another (Hanson and Jones 1998); and 3) Olivine from reduced basaltic liquids (fO_2 < FMQ) contains vanishingly small quantities of Fe^{3+} (Canil and O'Neill 1996), mitigating issues associated with the temperature-dependent electron exchange reaction between Cr^{2+} and Fe^{3+} that is responsible for affecting the equilibrium Cr^{3+}/Cr^{2+} in the melt. In this way, olivine crystals can effectively record the Cr^{3+}/Cr^{2+} of their parental liquids, in much the same way as melt inclusions record the composition of the melt from which a particular crystal grew.

Experimental techniques and analytical methods

Experimental techniques

Wire loop experiments were conducted in the one-bar gas mixing laboratory at NASA Johnson Space Center (JSC). The majority of the experiments were performed using Re loops to prevent Fe-loss. Experiments run at oxygen fugacities near the FMQ buffer employed Pt-Rh loops. The starting materials consisted of two compositions patterned after the whole rock composition of Martian meteorite Yamato 980459. Both compositions consisted of a mixture of synthetic oxides. One of these compositions was doped with REE, whereas the other was a REE-free base composition. The REEs were added to the doped composition as 0.6% of their

individual oxides, to yield a total abundance of ~4.5 wt. % REE-oxide. Scandium and vandium were also added to this mixture as Sc_2O_3 and V_2O_3 at a concentration of 0.1 wt. % each. We recognize that the doping levels employed in this study do not realistically approximate the actual Y-98 bulk composition; however, such elevated concentrations of trace elements are required for future XANES measurements of the valence states of other important trace elements. The experiments presented here are part of a larger, ongoing phase equilibrium and partitioning study that focuses on compositions of martian basaltic liquids.

Experiments were performed at temperatures of 1300˚C, 1320˚C and 1380˚C. The 1300˚C experiments utilized the doped composition (Y-98A series), whereas the 1320˚C (Y-98B797 & B791) and 1380˚C (Y-98B796 & B790) experiments used the un-doped starting mixture. Experimental fO_2 was controlled with CO-CO_2 mixtures that were calibrated with a Y-stabilized zirconia electrochemical oxygen sensor, specifically the $SIRO_2$ from COF-Australia, housed in a dedicated reference furnace. Experimental runs were conducted at the following relative fO_2 values: IW-1, IW, IW+1, and IW+3.4 (=FMQ) for the 1300˚C series of REE-doped experiments, and IW-1 and IW+3.4 for the un-doped 1320˚C and 1380˚C experiments. Each experiment was initially held at super-liquidus conditions (1500˚C) for eight hours and subsequently cooled to target dwell temperature at a rate of 1000˚C hr^{-1}. The liquidus for the Y-98 composition has been determined to be approximately 1420˚C at 1 bar (Musselwhite et al. 2006). Experiments were held at the target dwell temperature for a minimum of 48 hours and terminated by drop-quenching into distilled water.

Electron microprobe analysis (EPMA) of the experimental glasses and olivine

Electron microprobe (EPMA) analyses were conducted using the JEOL JXA 8200 electron microprobe in the Institute of Meteoritics at the University of New Mexico. Quantitative

119 analyses were collected for Si, P, Al, Fe, Ti, Cr, Ca, Na, K, Mn, and Mg at an accelerating
120 voltage of 15 kV, a beam current of 10 nA, and a 1 μm spot size. Standardization was carried out
121 using a combination of CM Taylor electron microprobe mineral standards, specifically
122 orthoclase, albite, diopside, olivine, spessartine, apatite, and chromite, as well as –in-house
123 standards for rutile, almandine, and fayalite. All data were reduced with a ZAF matrix correction
124 algorithm within the JEOL software. Care was taken to ensure that chosen spots were a
125 significant distance (typically >100 μm) away from any Cr-spinel inclusions in the olivine or
126 glass to mitigate potential enhancement of the apparent Cr content of olivine and glass resulting
127 from Cr secondary fluorescence originating from Cr-spinel crystals.

128 **X-ray absorption near edge spectroscopy (XANES) data acquisition and reduction**

129 Chromium K-edge XANES data were acquired with the x-ray microprobe of GSECARS
130 beamline 13-ID-E at the Advanced Photon Source (APS), Argonne National Laboratory, Illinois.
131 The x-ray source at APS beamline 13-ID-E was a 72-pole, 33 mm period undulator. Beam
132 focusing was accomplished with dynamically-figured Kirkpatrick-Baez focusing mirrors; this
133 configuration yielded a beam focused to a final spot size of ~ 4 μm^2. All spectra were acquired in
134 fluorescence mode utilizing a cryogenically cooled Si(311) monochromater and a silicon-drift
135 solid state detector offset at a 45° angle from the sample. Spectra were collected through the
136 energy range of 5939 eV - 6213 eV. The energy step width was set to 0.2 eV in the near edge
137 region (5984 eV to 6014 eV) and to 4.0 eV in the far pre-edge and far post-edge regions. Data
138 acquisition consisted of two spectral sweeps per spot analysis. The two resultant spectra were
139 subsequently merged into a single spectrum in order to maximize signal-to-noise. Multiple
140 olivine crystals were analyzed in each experimental charge. Locations for the analytical spots
141 were purposefully selected to sample both the core and rim of the olivine crystal in an attempt to

assess the homogeneity of the Cr valence within individual olivine phenocrysts. A total of four to five olivine spot analyses were obtained for each experimental charge. Two standards were used to define the Cr-valence end-members. The Cr^{3+} standard was an iron-free glass produced experimentally in the study of Hanson and Jones (1998), and the Cr^{2+} was a Cr-bearing ureilite olivine that was previously characterized by Goodrich et al. (2012).

The formal oxidation state of Cr has been shown to correlate with the intensity of a shoulder on the main Cr-K absorption edge (Berry and O'Neill 2004). Existence of this spectral feature at ~5994 eV has been attributed to a 1s-4s electron transition (Sutton et al. 1993). The 1s-4s electron transition is forbidden for cations in non-centrosymmetric coordination polyhedra, however, with respect to Cr^{2+} in octahedral coordination, the Jahn-Teller effect causes symmetry-braking site distortion making 1s-4s transition permissible (in contrast, the Jahn Teller effect for Cr^{3+} in octahedral coordination is negligible). Therefore, the 1s-4s absorption at ~5994 eV is diagnostic of the presence of Cr^{2+} in the olivine structure. The intensity of the 1s-4s shoulder at ~5994 eV has been shown to be directly correlated with the abundance of divalent Cr present in the olivine relative to trivalent Cr (Berry and O'Neill 2004). Data reduction and calculation of Cr^{2+}/Cr^{3+} values followed the general procedures outlined in the work of Berry and O'Neill (2004). Both of these works conclude that both the area and the intensity of the spectral feature associated with 1s-4s electron transition are correlated with the Cr^{2+} content of the olivine.

Figure 1 is a stack plot of representative Cr spectra, including both standards and some examples from the olivine crystals from the Y-98A experiments. The normalized spectra were first smoothed with a three iteration moving average, and then differentiated to obtain the final processed spectra. The derivatives of the normalized intensity spectra help facilitate the accurate

calculation of the intensity of the absorption associated with the 1s-4s transition. In the derivative spectra, the 1s-4s transition is prominently manifested as a single peak roughly centered about 5994.5 eV (Figure 2). The valence ratios for unknown olivine crystals were obtained using the linear mixing line between the 1s-4s intensity of the Cr^{3+} standard (defined as $Cr^{2+}/\Sigma Cr = 0$) and the equivalent intensity for the Cr^{2+} standard (defined as $Cr^{2+}/\Sigma Cr = 0.95$). Intensities of the 1s-4s transition calculated from the derivative spectra as well as their corresponding Cr^{2+}/Cr^{3+} values are listed in Table 1. Calculations of $Cr^{2+}/\Sigma Cr$ presented in this study were made with the simple intensity (height) of the 1s-4s peaks in the derivative spectra (Table 1).

For comparison, we have also calculated $Cr^{2+}/\Sigma Cr$ of the unknown olivine using the area of the 1s-4s peaks from the derivative spectra. Intensities calculated with this data reduction scheme were obtained through the numerical integration of the derivative spectra over an energy interval from 5991.5 eV to 5995 eV. The area of the peak obtained through the integration (i.e., the integrated intensity) scales with $Cr^{2+}/\Sigma Cr$ of the standards in a manner nearly identical to the relationship between the peak height and $Cr^{2+}/\Sigma Cr$. The olivine $Cr^{2+}/\Sigma Cr$ values obtained using the integrated area reduction scheme are nearly identical to those calculated using the peak height, suggesting that both methods render robust Cr valence data.

Based on replicate measurements, we estimate that the inherent uncertainty associated with the measured $Cr^{2+}/\Sigma Cr$ values is approximately ± 0.05 (1σ). We also recognize that crystallographic orientation can affect the measured intensity of the 1s-4s absorption The orientation effect is about ± 10% of the Cr^{2+} peak intensity which corresponds to a maximum valence uncertainty of ± 0.1 for a sample containing only Cr^{2+} (Sutton et al. 2013 *in review*). These observations indicate that significant orientation effects are only manifested in materials containing high $Cr^{2+}/\Sigma Cr$.

Results

The compositions of the quenched liquid and olivine

All experimental run products consisted of some combination of quenched liquid, olivine, and Cr-enriched spinel. The phase assemblages for each experiment are also listed in Table 1. In order to assess whether or not the experiments attained equilibrium, we have examined the olivine-liquid Fe-Mg exchange K_d values. The calculated K_d values for experimental olivine-liquid pairs range from 0.32 to 0.35, suggesting that the olivine has indeed approached compositional equilibrium with the liquid (Roeder and Emslie, 1970; Filliberto and Dasgupta 2011). Inter-experiment variation in the major element composition of the olivine is very low, such that all of the analyzed olivine crystals from the Y-98A experiments fall within compositional range Fo_{77} to Fo_{81}, and all of the olivine crystals from the Y-98B experiments fall within the compositional range Fo_{82} to $Fo_{86.}$ The compositions of the olivine and glass from all of the experimental charges are supplied in Electronic Appendix I and Electronic Appendix II. The low variability in the Fe/Mg ratios of the experimental olivine, however, are not unanticipated as the low ferric iron contents of all the experimental melts severely limit any variation in the ratio of activities of FeO and MgO. Calculations using the Kress and Carmichael (1991) equation support this interpretation by indicating that the maximum $Fe^{3+}/\Sigma Fe$ is ~ 0.12, even for the most oxidized experimental liquids.

The EPMA-determined Cr_2O_3 content (reported in Table 1 as ppm elemental Cr) of the quenched Y-98A series liquids ranged from a high of 6300 ± 300 ppm (1σ) at IW-1, monotonically decreasing to a low of 2550 ± 236 ppm (1σ) at IW+3.4. A similar trend is observed for the liquids resulting from the Y-98B experiments. In the 1320˚C experiments, the Cr content drops from 8150 ± 290 ppm at IW-1 to 3310 ± 330 ppm at IW+3.4; in the 1380˚C

experiments, Cr content decreases from 7920 ± 430 ppm at IW-1 to 4790 ± 420 ppm at FMQ. We interpret the monotonic decrease in the Cr content of the quenched liquids as an effect of the increasing modal abundance of Cr-spinel in the more oxidized experiments. The early crystallization of Cr-rich spinel depletes the residual liquid of Cr in the more oxidized charges. As expected, the Cr content of the olivine that crystallized from the liquids also decreased from a high of 4300 ± 225 ppm (1σ) at IW-1 to a low of 1500 ± 200 ppm (1σ) at FMQ in an analogous, monotonic fashion. The Cr content of the olivine in both sets of Y-98B experiments mirrors the trend observed for the Y98-A series. Cr content of both the liquid and olivine are plotted vs. fO_2 in Figure 3a.

Total Cr partition coefficients

The calculated total Cr partition coefficients for olivine-liquid pairs range from 0.59 to 0.72. Both the 1300°C and the 1320°C experiments show some systematic variation of the D_{Cr} with fO_2. In contrast, the high temperature Y-98B experiments yield a D_{Cr} that is constant with respect to fO_2. The bulk D_{Cr} values are plotted vs. fO_2 in Figure 3b. The apparent effect of fO_2 on D_{Cr} in the lower temperature experiments will be addressed in detail in the discussion section below. Propagated 1σ uncertainties for the partition coefficient values are approximately ± 0.09. The olivine-liquid partition coefficients calculated in this study are in excellent agreement with the values derived from multiple experimental Cr partitioning studies (Mikouchi et al. 1994, Gaetani and Grove 1997, Hanson and Jones 1998, and Mallmann and O'Neill 2009). Results of studies at comparable temperatures (1300˚C-1400˚C) unanimously suggest that the D_{Cr} value falls between 0.55 and 0.85, a range consistent with the range of values from this study. The reader should bear in mind that the liquids from previous studies span a fairly large compositional range, many of which have stark differences from the liquid compositions encountered in this study.

XANES measurements of Cr valence in olivine

The measured $Cr^{2+}/\Sigma Cr$ values from individual olivine spot analyses display a relatively large range, varying from a low of 0.26 to a high of 0.90. Dispersion, as measured using the 1σ standard deviation, in the $Cr^{2+}/\Sigma Cr$ within single experiments is generally low. The standard deviation of the $Cr^{2+}/\Sigma Cr$ values within a single experimental charge is approximately 0.03 in the IW, IW+1 and IW+3.4 experiments, and 0.09 in the IW-1 experiment. The measured $Cr^{2+}/\Sigma Cr$ values for the olivine in the IW-1 Y-98A experiments range from 0.74 to 0.90. Normalized XANES spectra from all experiments have been supplied in Electronic Appendix III.

The dispersions displayed in these analyses are likely a reflection of orientation effects, as orientation effects are most strongly realized in olivine with high $Cr^{2+}/\Sigma Cr$. This is consistent with the observation that olivine in the most reduced experiments contains not only the largest quantity of Cr^{2+}, but also show the largest spread in calculated $Cr^{2+}/\Sigma Cr$ values. Therefore, the mean of these values represents a more accurate reflection of the actual $Cr^{2+}/\Sigma Cr$ present in the olivine than any of the individual analyses. The fact that the mean $Cr^{2+}/\Sigma Cr$ of 0.82 yields a regression slope of 0.24 in a plot of $\ln[Cr^{3+}/Cr^{2+}]$ vs. $\ln fO_2$ is strong evidence that the mean value is indeed an accurate measure of $Cr^{2+}/\Sigma Cr$ for this experiment.

Figure 4 is a plot of the $Cr^{2+}/\Sigma Cr$ vs. $\log_{10} fO_2$; this plot clearly shows that Cr^{2+} comprises an increasing proportion of the total Cr content in the olivine as the experimental oxygen fugacity is lowered. As a first order observation, the calculated $Cr^{2+}/\Sigma Cr$ values show a distinct trend as a function of the experimental fO_2 values. The trend in the data suggests that the Cr valence ratio in the olivine is indeed sensitive to the oxidation state of the experimental charge and, by extension, the oxidation state of the melt from which the crystals in question nucleated and grew. The

256 quantitative links between the measured Cr valence ratio in the experimental olivine and the
257 valence ratio of its parental melt will be explored in detail in the next section.
258
259 **Discussion**
260 **Relationship of Cr valence ratio in olivine to the Cr valence ratio of the melt**
261 The measured $Cr^{2+}/\Sigma Cr$ of olivine can be quantitatively related to the $Cr^{2+}/\Sigma Cr$ of its parental
262 liquid through the olivine-melt partition coefficients for both divalent and trivalent chromium. In
263 other words, the ratio of Cr^{3+} to Cr^{2+} in olivine is defined by the ratio of Cr^{3+} to Cr^{2+} in its
264 parental liquid, multiplied by a factor equal to the ratio of D_{Cr}^{3+} to D_{Cr}^{2+}. This relationship is
265 defined by Eq. 1.
266
267 Eq. 1 $$\left(\frac{XCr^{3+}}{XCr^{2+}}\right)^{olivine} = \left(\frac{XCr^{3+}}{XCr^{2+}}\right)^{liquid} \circ \left(\frac{D_{Cr^{3+}}^{ol-liq}}{D_{Cr^{2+}}^{ol-liq}}\right)$$
268
269 where XCr^{3+} and XCr^{2+} represent the mole fraction of that cation present in a given phase and
270 D_{Cr}^{2+} and D_{Cr}^{3+} represent the olivine liquid Nernst-type partition coefficients for divalent and
271 trivalent Cr, respectively. From a practical standpoint, Cr^{3+}/Cr^{2+} of any olivine-bearing melt can
272 be inferred from direct measurements of the Cr^{3+}/Cr^{2+} present in its olivine phenocrysts;
273 however, this relationship is only useful provided that the ratio of Cr partition coefficients for
274 (trivalent to divalent) are known with sufficient accuracy. Fortunately, for many common
275 basaltic compositions, the partition coefficient ratio for Cr^{2+} and Cr^{3+} is closely approximated to
276 be a constant with a value of approximately 1.0. This may not be the case for all basaltic melt
277 compositions, however (Hanson and Jones 1998).

In order to calculate the individual values for D_{Cr}^{3+} and D_{Cr}^{2+}, knowledge of the molar ratio of Cr^{3+}/Cr^{2+} in both the olivine and the quenched liquid is required. This is not possible for the experiments in this study because of the difficulties associated with quench modification of the Cr^{3+}/Cr^{2+} in the high fO_2, iron-rich experimental liquids. A simple analysis of the bulk D_{Cr} behavior was used to circumvent this obstacle. This test consists of a comparison of the bulk olivine-liquid partition coefficients from experiments performed at different oxygen fugacity values. Upon close examination, the bulk D_{Cr} values slightly deviate from a constant value as fO_2 is increased. The calculated values become slightly lower, decreasing from 0.70 to 0.59 as fO_2 is increased from IW-1 to FMQ. This behavior is observed in both the doped 1300˚C and un-doped 1320˚C series experiments. The subtle decrease of the bulk D_{Cr} values may be interpreted in two different ways:

1) One or both of the individual partition coefficients that comprise the bulk D_{Cr} vary as a function of fO_2 in a manner that yields a non-constant ratio of D values; or

2) The individual partition coefficient values for Cr^{3+} and Cr^{2+} are fixed with a trivalent to divalent ratio less than one.

Although these possibilities may appear similar on the surface, each has very different implications for the geochemical behavior of Cr in basaltic magmas. The first interpretation suggests that the behavior of Cr^{3+} and Cr^{2+} oxide components are governed by rather complex thermodynamic relationships. Such behavior implies that as the relative abundances of trivalent and divalent Cr change in the liquid with either increasing or decreasing fO_2, the bonding

behavior and speciation of these components in the liquid must be substantially altered. In other words, this interpretation requires that the activities of $CrO_{1.5}$ and CrO in the liquid are variable with respect to fO_2; however the work of Berry and O'Neill (2004) directly contradicts this interpretation. Berry and O'Neill (2004) concluded that the activity coefficient ratio ($\gamma Cr^{3+}/\gamma Cr^{2+}$) is, in fact, invariant with respect to fO_2 in liquids of constant bulk composition and sufficiently dilute total Cr contents (< 1.0 wt. %). The total Cr content of the melts in all experimental charges of this study is sufficiently dilute so as to display activity composition relationships that comply with Henry's Law. Furthermore, differences in the major element composition of the liquid in experiments run at differing oxygen fugacity values are minimal and therefore cannot explain the variation in the bulk D_{Cr} with fO_2.

The second interpretation offers a parsimonious explanation that is consistent with the conclusions of Berry and O'Neill (2004). This interpretation simply requires that the partition coefficient for Cr^{3+} be slightly less than that for Cr^{2+}. Olivine crystalized from liquids in systems that follow such partitioning behavior must have $Cr^{2+}/\Sigma Cr$ that is greater than the liquid. The most important consequence is that this interpretation requires bulk D_{Cr} to be a function of the fO_2 of the liquid. The observed trend in bulk D_{Cr} vs. fO_2 can (Figure 3b) can be reproduced if the ratio of $D_{Cr}^{3+}$to D_{Cr}^{2+} is approximately 0.80 (see Eq. 1). In this case, the value of the partition coefficient ratio is a simple manifestation of the fact that divalent Cr is preferred in the olivine structure over trivalent Cr. This interpretation implicitly requires that the crystal chemistry of the olivine dictate the variation of D_{Cr} with fO_2, rather than non-Henrian behavior where CrO and $CrO_{1.5}$ display oxygen fugacity-dependent activity coefficients. It is, however, notable that the D_{Cr} values for the two Y98B experiments conducted at 1380˚C show little variation as a function of fO_2. This observation suggests that the ratio of $D_{Cr}^{3+}$to D_{Cr}^{2+} in the higher temperature

experiments may be closer to ~1.0, however, considering that only two experiments were conducted at this temperature it is difficult to fully vet this conclusion. We have chosen to use a D_{Cr}^{3+} to D_{Cr}^{2+} ratio 0.80 to calculate the $Cr^{2+}/\Sigma Cr$ of the experimental liquids. Because the application of the correct D_{Cr}^{3+} to D_{Cr}^{2+} ratio is critical to obtaining accurate $Cr^{2+}/\Sigma Cr$ for the liquid we have also calculated the $Cr^{2+}/\Sigma Cr$ of the Y98B 1380˚C experiments with D_{Cr}^{3+}/D_{Cr}^{2+} 1.0. We found that calculating the $Cr^{2+}/\Sigma Cr$ values for Y98B (1380˚C) liquids with a D_{Cr}^{3+} to D_{Cr}^{2+} ratio of 1.0 did not substantially change shift the modeled Cr valence ratios (Figures 7 and 8) presented later in this work. Therefore, we assert that applying a single correction factor of 0.80 to all of the experiments is the most justifiable treatment of the D_{Cr} data.

A plot of the corrected $\ln[Cr^{3+}/Cr^{2+}]$ values vs. $\ln fO_2$ yields a linear array of points for the Y-98A experiments and both Y-98B series experiments (Figure 5). For the Y-98A experiments a plot of the average corrected $\ln[Cr^{3+}/Cr^{2+}]$ vs. $\ln fO_2$ yields a linear array of points. Fitting the liquid-corrected data via linear regression yields a line with a slope of 0.24 and a correlation coefficient of $R^2 = 0.97$. The observed relationship between $\ln[Cr^{3+}/Cr^{2+}]$ and $\ln fO_2$ in the Y-98B experiments is consistent with that of the Y-98A experiments, which is somewhat surprising considering the intrinsic errors associated with the measurements, and that experiments from only two fO_2 values (IW-1 and IW+3.4) are represented. The regressed slopes of $\ln[Cr^{3+}/Cr^{2+}]$ vs. $\ln fO_2$ for the the un-doped Y-98B experiments are 0.21 and 0.23 for the 1320˚C and 1380 ˚C experiments, respectively.

Crystal chemical aspects controlling Cr partitioning into olivine

The fidelity of olivine as a recorder of Cr valence in the parent liquid hinges on the fact that the compatibility of Cr^{2+} and Cr^{3+} are approximately equal in the olivine structure. For example, if the olivine/liquid partition coefficients for divalent and trivalent Cr were different by a factor

of five, it would greatly restrict the fO_2 range over which Cr could have multiple valences in olivine. Therefore, the question of why Cr^{3+} is so compatible (relative to Cr^{2+}) must be reconciled with the crystal chemistry of olivine, and any observed trends in Cr partitioning behavior must be consistent with known crystal chemical constraints. A few qualitative explanations of Cr behavior in olivine are offered in the next paragraph.

Hanson and Jones (1998) suggest that while Cr^{2+} is the correct charge, its radius is a bit too large to be compatible in the olivine crystal structure; for Cr^{3+}, the opposite is true: its charge is too large, but its radius is nearly identical to that of Mg^{2+}. As far as charge balance for Cr^{3+} in the olivine lattice is concerned, existing data suggest that either Al^{3+} (in the tetrahedral site) nor Na^{+} (in one of the octahedral sites) act as a significant charge couple for Cr^{3+} unless pressures exceed 3GPa (Taura et al. 1998). These data suggest that at lower pressures, vacancy-based substitutions must be required for charge balance. Hanson and Jones (1998) and Papike et al. (2005) both suggested that the mechanism by which Cr^{3+} is accommodated at low pressures may be a vacancy substitution where two Cr^{3+} substitute for three Mg^{2+} cations and a vacancy:

$$2\,{}^{VI}Cr^{+3} + {}^{VI}\square \leftrightarrow 3\,{}^{VI}Mg^{+2}$$

$$2\,{}^{VI}Cr^{+3} + {}^{VI}\square \leftrightarrow 3\,{}^{VI}Fe^{+2}$$

yielding the olivine formula units $Cr(Mg_{0.5}\square_{0.5})SiO_4$ and $Cr(Fe_{0.5}\square_{0.5})SiO_4$, respectively. The nature of the substitution mechanism is important because the partitioning behavior for Cr^{3+} is decoupled from the presence of other charge-balancing cations within the olivine structure. Rather than Cr compatibility scaling with the vacancy density of the olivine, the presence of Cr^{3+} in olivine partially controls the vacancy density of the olivine.

369

370 **Thermodynamics of Cr redox equilibria in the melt**

371 If the $Cr^{2+}/\Sigma Cr$ measured in olivine does indeed reflect that of the liquid, then it must be
372 consistent with the Cr redox behavior observed for liquids from other studies of Cr redox
373 systematics. The $Cr^{2+}/\Sigma Cr$ observed in olivine can be defined by the homogenous redox
374 equilibrium between divalent and trivalent Cr in the melt (cast here as the oxide components CrO
375 and $CrO_{1.5}$):

376

377 Eq.2 $$CrO^{liq} + \tfrac{1}{4} O_2^{sys} = CrO_{1.5}^{liq}$$

378

379 or it can be defined in standard thermodynamic notation as:

380

381

382 Eq. 3 $$ln\left(\frac{XCrO_{1.5}}{XCrO}\right)^{liq} = \tfrac{1}{4} ln fO_2 - ln\left(\frac{\gamma CrO_{1.5}}{\gamma XCrO}\right) + \frac{\Delta G^{\circ}_{rxn}}{-RT}$$

383

384 The olivine Cr^{3+}/Cr^{2+} values determined from the XANES measurements can be translated into
385 the Cr^{3+}/Cr^{2+} of the melt by re-arranging and substituting Eq. 1 into the expression above (Eq.3),
386 using the partition coefficient ratios derived in the Discussion section.

387 We have calculated the empirical equilibrium constant logK' for the homogenous CrO-$CrO_{1.5}$
388 equilibrium with the olivine derived $Cr^{2+}/\Sigma Cr$ values of the melt, where logK' by definition
389 includes the $\ln[\gamma CrO_{1.5}/\gamma CrO]$ term from Eq. 3. The logK' values determined from this study
390 overlap those determined by Berry et al. (2006) and, considering the effects of temperature and
391 composition, the results are in excellent agreement. Figure 6 shows the logK' values from this

study plotted vs. logfO_2, as well as a few values from the Berry et al. (2006) data set. It is important to note that logK' values for all of the Y-98A series experiments are constant with respect to fO_2. This observation corroborates the assumption that melts with dilute Cr contents display Henrian behavior (i.e. fO_2 invariant $\gamma CrO/\gamma CrO_{1.5}$), as made in Berry and O'Neill (2004) and Berry et al. (2006). The identical logK' values for the REE doped Y-98A (1300˚C) and un-doped Y-98B (1320˚C) experiments suggest that the presence of the REE do not fundamentally affect the observed Cr redox systematics, at least within the resolution with which $Cr^{2+}/\Sigma Cr$ can be measured.

A comparison of the logK' values from the 1300˚C Y-98A and 1320˚C Y-98B experiments with the logK' values the 1380˚C experiments clearly indicates that increasing temperature at constant fO_2 (relative to a buffer) depresses logK'. Or in other words, increased temperature translates to an increased $Cr^{2+}/\Sigma Cr$ at constant fO_2 in the Y-98 liquids. The effects of temperature on the logK' are caused by the individual effects of temperature on the ΔG° of the equilibrium in Eq. 2 and the effects of temperature on the activity coefficient ratio, $\gamma CrO_{1.5}/\gamma CrO$. Unfortunately these two effects cannot be disentangled from one another, as no thermodynamic data exist with which to calculate the ΔG° of the Cr redox equilibrium as a function of temperature. That said, it is unlikely that temperature affects the ΔG° and not the $\gamma CrO_{1.5}/\gamma CrO$. Partitioning data from Hanson and Jones (1998) support this interpretation by showing that D_{Cr2+} is a function of temperature; this observation implies that the γCrO of the melt is indeed a function of temperature.

Small differences between the logK' values of the Y-98 experiments and those from the Berry et al. (2006) study (Figure 6) arise naturally because of differences in melt compositions and temperature. All of the compositions investigated by Berry et al. were restricted to the CMAS

system at temperatures of 1400˚C. Most of the difference between the Berry and O'Neill logK' values and those from the 1300˚C Y-98A and 1320˚C Y-98B experiments can be attributed to the differences in temperature. The higher logK' values (~2.3) associated with the 1300˚C Y-98A and 1320˚C Y-98B experiments are consistent with the observation that decreasing temperature causes an increase in logK'. In contrast, the logK' values calculated for the 1380˚C Y-98B experiments are strikingly similar to those reported in the Berry et al. data set. The logK' values from the 1380˚C Y-98B experiments fall between the AnDi+Fo and AnDi+Wo (where AnDi = anorthite-diopside) compositions from Berry et al. (2006). This suggests that at approximately 1400˚C, the $\gamma CrO_{1.5}/\gamma CrO$ for the Y-98 composition must lie somewhere between the $\gamma CrO_{1.5}/\gamma CrO$ values of anorthite-diopside + foresterite (AnDi+Fo) and anorthite-diopside + wollastonite (AnDi+Wo) compositions from Berry et al. (2006).

Using the logK' values calculated for the melts in this study, it is possible to construct a model curve of $Cr^{2+}/\Sigma Cr$ as a function of fO_2 and the K' values for melts of Y-98 bulk composition:

Eq. 4
$$\frac{XCr^{2+}}{\Sigma Cr} = \left[1 + e^{\left(\frac{1}{4} ln fO_2 + lnK'\right)}\right]^{-1}$$

Figure 7 contains plots of the modeled $Cr^{2+}/\Sigma Cr$ values for Y-98 liquids at 1300˚C. Our modeling indicates that the $Cr^{2+}/\Sigma Cr$ value for a Y-98 liquid at 1300˚C varies from 0.65 at IW to 0.53 at IW+1.5. Similarly the modeled $Cr^{2+}/\Sigma Cr$ values for 1380˚C vary from 0.89 at IW to 0.77 at IW+1.5. This modeling places important constraints on the manner in which temperature affects equilibrium $Cr^{2+}/\Sigma Cr$ in planetary basalts. Figure 8 illustrates the effects of temperature on the homogenous Cr redox equilibrium with a plot of the modeled Cr redox curves at 1300˚C

and 1380˚C. With increasing temperature there is a prominent displacement of the center of the sigmoidal curve (i.e. the point corresponding to an equal mixture of Cr^{2+} and Cr^{3+}) to higher fO_2 values. To the first order, increasing temperature for the Y-98 bulk composition appears to cause the reduction of Cr^{3+} to Cr^{2+} at a constant fO_2 value (defined relative to a buffer). The model curves indicate that an 8.5 % reduction in the $Cr^{2+}/\Sigma Cr$ of the melt is caused by simply increasing the temperature of the system 80˚C.

Conclusions and implications for the natural Y-98 melt

The results of this study demonstrate that $Cr^{2+}/\Sigma Cr$ systematically changes with the oxidation state of its equilibrium melt. Measured $Cr^{2+}/\Sigma Cr$ can be translated to the $Cr^{2+}/\Sigma Cr$ of the melt if the ratio of D_{Cr}^{3+} to D_{Cr}^{2+} is well known for the system of interest. Ratios of D_{Cr}^{3+} to D_{Cr}^{2+} are not canonical, but rather vary with temperature and melt composition. The systematic variation of Cr oxidation state in olivine with fO_2 can be viewed in two lights: 1) as a calibration Cr valence that is a function of fO_2 and directly applicable to Y-98 melts, or 2) as a general method for estimating Cr^{3+}/Cr^{2+} of the melt from which the olivine crystal grew. For the latter to be useful, a comprehensive understanding of Cr redox systematics as a function of composition, temperature, and pressure is required. If more data were available, K' could potentially be cast as a function of P-T-X, potentially making the $Cr^{2+}/\Sigma Cr$ measurements in olivine applicable to any melt composition. In either case, measurements of $Cr^{2+}/\Sigma Cr$ olivine that was crystallized from primitive mantle derived melts can yield important insights into the equilibrium ratio of $Cr^{2+}/\Sigma Cr$ that was present in these melts. Furthermore, such measurements may allow for the calculation of the oxidation state of the magmas and potentially that of their mantle source regions. Specifically, Cr redox measurements from this study have derived valuable estimates of the K'

for the homogenous $CrO_{1.5}$-CrO equilibrium in a composition representing a primitive, iron-rich martian basalt. Future efforts concentrating on constraining the effects of pressure on the homogenous Cr redox equilibrium may provide more important insight into the $Cr^{2+}/\Sigma Cr$ redox ratio of the earliest partial mantle melts.

Assuming the effects of pressure on the Cr redox equilibrium are minimal (in the absence of data), results from this work also suggest that the primitive Y-98 melt may have contained significant quantities of both trivalent and divalent chromium at temperatures below 1380˚C. Interestingly, this conclusion places the valence ratio of Cr in martian basalts somewhere in between that of the Moon (highly Cr^{2+} enriched) and that of the Earth (highly Cr^{3+} enriched). The $Cr^{2+}/\Sigma Cr$ of the melt can also change substantially as a function of temperature without a concomitant change in the fO_2 of the melt. Given a constant relative fO_2 value, melts at higher temperatures appear more reduced with respect to their $Cr^{2+}/\Sigma Cr$ than that of the same melt composition at a lower temperature. This observation importantly suggests that Cr valence ratios in natural magmas must be interpreted in the context of an equilibration temperature. Finally, XANES-based measurements of $Cr^{2+}/\Sigma Cr$ in olivine can potentially be used as an fO_2 sensor, provided that the olivine crystallization temperature and K' for the composition of interest are known.

Acknowledgements

This research was supported by NASA Cosmochemistry grants to C. Shearer and J. Jones. Francis McCubbin is also thanked an early, informal review of the manuscript. Steve Simon and Fred Davis are thanked for reviews that improved the content and the readability of the manuscript. We gratefully acknowledge the beamline award, as well as assistance of GSECARS beamline staff. GeoSoilEnviroCARS is supported by the National Science Foundation-Earth Sciences (EAR-1128799) and Department Geosciences (DE-FG02-94ER14466). Use of the Advanced Photon Source was supported by U.S. Department of Energy. Office of Science. Office of Basic Energy Science under contract No. DE-AC02-06CH11357.

References

Arculus, R.J., Delano, J.W. (1981) Intrinsic oxygen fugacity measurements: techniques and results for spinels from upper mantle peridotites and megacryst assemblages. Geochimica et Cosmochimica Acta, 45, 899-913.

Ballhaus, C. (1993) Redox states of lithospheric and asthenospheric upper mantle. Contributions to Mineralogy and Petrology, 114, 331-348.

Berry A.J., O'Neill, H.StC. (2004) A XANES determination of the oxidation state of chromium in silicate glasses. American Mineralogist, 89, 790-798.

Berry AJ, O'Neill H. StC., Scott DR, Foran GJ, Shelley J. MG. (2006) The effect of composition on Cr^{2+}/Cr^{3+} in silicate melts. American Mineralogist, 91, 1901-1908.

Brandon, A.D., and Draper, D.S. (1996) Constraints on the origin of the oxidation state of mantle overlying subduction zones: an example from Simcoe, Washington, USA Geochimica et Cosmochimica Acta, 60, 1739 -1749.

Canil, D. (2002) Vanadium in peridotites, mantle redox state, and tectonic environment: Archean to present. Earth and Planetary Science Letters, 195, 75-90.

Canil, D. and O'Neill, H.St.C. (1996) Distribution of ferric iron in some upper mantle assemblages. Journal of Petrology, 37, 609–635.

Carmichael, I.S.E. (1991) The redox states of basic and silicic magmas: a reflection of their source regions? Contribions to Mineralogy and Petrology, 106, 129-141.

Delano, J.W. (1990) Experimental constraints on the oxidation state of the lunar mantle. Lunar and Planetary Science Conference Abstracts, XXI, 278-279.

Filiberto, J. and Dasgupta, R. (2011) Fe^{2+}–Mg partitioning between olivine and basaltic melts:

Applications to genesis of olivine-phyric shergottites and conditions of melting in the Martian interior. Earth and Planetary Science Letters, 304, 527-537.

Fudali, R.F. (1965) Oxygen fugacities of basaltic and andesitic magmas. Geochimica et Cosmochimica Acta, 29, 1063-1075.

Gaetani, G.A. and Grove, T.L. (1997) Partitioning of moderately siderophile elements among olivine, silicate melt, and sulfide melts: Constraints on core formation in the Earth and Mars. Geochimica et Cosmochimica Acta, 61, 1829- 1846.

Goodrich, C.A., Sutton, S.R., Wirick, S. (2012) Valences of Cr in Ureilite Olivine and Implications for Ureilite Petrogenesis. Lunar and Planetary Science Conference Abstracts, 43, 1221.

Hanson B., Jones J.H. (1998) The systematics of Cr^{3+} and Cr^{2+} partitioning between olivine and liquid in the presence of spinel. American Mineralogist, 83, 669-684.

Herd, C.D.K. (2003) The oxygen fugacity of olivine-phyric martian basalts and the components within the mantle and crust of Mars. Meteoritics and Planetary Science, 38, 1793-1805.

Irvine, T. N. (1975) Chromium: Its physiochemical behavior and petrologic significance. Geochimica et Cosmochimica Acta, 39, 779-780.

Karner, J.M., Papike, J.J., Sutton, S.R., Shearer, C. K., McKay, G., Le, L., and Burger, P. (2007) Valence state partitioning of Cr between pyroxene-melt: Effects of pyroxene and melt composition and direct determination of Cr valence states by XANES. American Mineralogist, 92, 2002-2005.

Kelley, K.A., and Cottrell, E. (2009) Water and the Oxidation State of Subduction Zone Magmas. Science, 325, 605-607.

Kress, V. C., and Carmichael, I. S. E. (1991). The compressibility of silicate liquids containing

534 Fe2O3 and the effect of composition, temperature, oxygen fugacity and pressure on their
535 redox states. Contributions to Mineralogy and Petrology, 108, 82-92.
536 Mackwell, S.J. (2008) Rheological Consequences of Redox State. Reviews in Mineralogy and
537 Geochemistry 68, 555-569.
538 Mallmann, G., O'Neill, H. StC. (2009) The crystal/melt partitioning of V during mantle melting
539 as a function of oxygen fugacity compared with some other elements (Al, P, Ca, Sc, Ti,
540 Cr, Fe, Ga, Y, Zr and Nb) Journal of Petrology, 50, 1765-1794.
541 Mathez, E.A. (1984) Influence of degassing on oxidation states of basaltic magmas. Nature, 310,
542 371-375
543 Mikouchi, T., McKay, G., and Le, L. (1994) Cr, Mn, and Ca distributions for olivine in angritic
544 systems: Constraints on the origins of Cr-rich and Ca-poor core olivine in angrite
545 LEW87051. Lunar and Planetary Science Conference Abstracts, XXV, 907-908.
546 Musselwhite, D.S., Dalton, H.A., Kieffer, W.S., and Treiman, A.H (2006) Experimental
547 petrology of the basaltic shergottite Yamato-980459: Implications for the thermal
548 structure of the Martian mantle. Meteoritics and Planetary Science, 41, 1271-1290.
549 O'Neill H.StC, Berry A.J. (2006) Activity coefficients at low dilution of CrO, NiO and CoO in
550 melts in the system CaO–MgO–Al2O3–SiO2 at 1400°C: Using the thermodynamic
551 behaviour of transition metal oxides in silicate melts to probe their structure. Chemical
552 Geology, 231, 77-89.
553 Papike, J.J. Karner, J., and Shearer, C.K. (2005) Comparative planetary mineralogy: Valence
554 state partitioning of Cr, Fe, Ti, and V among crystallographic sites in olivine, pyroxene,
555 and spinel from planetary basalts. American Mineralogist, 90, 277-290.
556 Righter, K. (2003) Metal-Silicate Partitioning of Siderophile Elements and Core formation in the

557 early Earth. Annual Review of Earth and Planetary Sciences, 31, 135-174.
558 Roeder, P.L., and Emslie, R.F. (1970) Olivine-liquid Equilibrium. Contributions to Mineralogy
559 and Petrology, 29, 275-289.
560 Shearer, C.K., McKay, G., Papike, J.J., and Karner, J.M. (2006) Valence state partitioning of
561 vanadium between olivine-liquid: Estimates of the oxygen fugacity of Y980459 and
562 application to other olivine-phyric martian basalts. American Mineralogist, 91, 1657-16
563 Schreiber, H.D., Haskin, L.A. (1976) Chromium in basalts: Experimental determination of
564 redox states and partitioning among synthetic silicate phases. Lunar and Planetary
565 Science, VII, 1221-1259.
566 Sutton, S.R., Jones, K.W., Gordon, B., Rivers, M.L., Bajt, S., and Smith, J.V. (1993) Reduced
567 chromium in olivine grains from lunar basalt 15555: X-ray absorption near edge structure
568 (XANES). Geochimica et Cosmochimica Acta, 57, 461-468.
569 Taura, H., Yurimoto, H., Kurita, K., and Sueno, S. (1998) Pressure dependence of partition
570 coefficients for trace elements between olivine and the coexisting melts. Physics and
571 Chemistry of Minerals, 25, 469-484.
572 Wadhwa, M. (2001) Redox state of Mars' upper mantle from Eu anomalies in shergottite
573 pyroxene. Science, 292, 1527-1530.
574 Wood, B.J., Bryndzia, L.T, and Johnson, K.E. (1990) Mantle oxidation state and its relation to
575 tectonic environment and fluid speciation. Science, 248, 337-345.
576
577
578
579

580 **Table 1 XANES Data and Cr Contents of Olivine and Melt**

Sample ID	$\log_{10} fO_2$	Int. 1s-4s[1]	B-line Cor[2]	$Cr^{2+}/\Sigma Cr$	Phases	Cr olivine[3]	Cr liquid[3]
Cr^{3+} H&J Glass	--	0.0176	NA	0.000	NA	NA	NA
Cr^{2+} Ureilite	--	0.1754	NA	0.950	NA	NA	NA
Y98-A10	-7.25	0.0668	0.04923	0.267	Liq, Ol, Spinel	1060 (135)	1750 (165)
	(IW+3.4)	0.0724	0.05483	0.297			
		0.0703	0.05272	0.286			
		0.0712	0.05363	0.290			
Y98-A2	-9.59	0.1076	0.09	0.487	Liq, Ol, Spinel	2086 (120)	2970 (125)
	(IW+1)	0.1121	0.0945	0.512			
		0.1086	0.091	0.493			
		0.1111	0.0935	0.506			
Y98-A14	-10.59	0.1366	0.119	0.645	Liq, Ol	2940 (205)	4280 (300)
	(IW)	0.1420	0.1244	0.674			
		0.1392	0.1216	0.659			
Y98-A17	-11.59	0.1538	0.1362	0.738	Liq, Ol	2950 (150)	4310 (205)
	(IW-1)	0.1848	0.1672	0.906			
		0.1522	0.1346	0.729			
		0.1842	0.1666	0.902			
Y98-B797	-11.39	0.1600	0.1424	0.771	Liq, Ol	4000 (190)	5575 (200)
	(IW-1)	0.1510	0.1334	0.723			
		0.1570	0.1394	0.755			
		0.1590	0.1414	0.766			
Y98-B791	-7.06	0.0690	0.0514	0.278	Liq, Ol, Spinel	1340 (250)	2265 (225)
	(IW+3.4)	0.0665	0.0489	0.265			
		0.0670	0.0494	0.268			
		0.0716	0.054	0.292			
Y98-B796	-10.8	0.1600	0.1424	0.771	Liq, Ol	3400 (190)	5420 (295)
	(IW-1)	0.1700	0.1524	0.825			
		0.1730	0.1554	0.842			
Y98-B790	-6.45	0.0731	0.0555	0.301	Liq, Ol, Spinel	2025 (340)	3270 (290)
	(IW+3.4)	0.0842	0.0666	0.361			
		0.0898	0.0722	0.391			

[1] data in the column are the raw intensities associated with the 1s-4s electron transition from the derivative spectra
[2] background subtracted intensities
[3]Cr content of the glass and olivine are reported in ppm of elemental Cr; the value following in ( ) is the 1σ uncertainty associated with the EPMA measured Cr contents
NA = not applicable

Figure 1

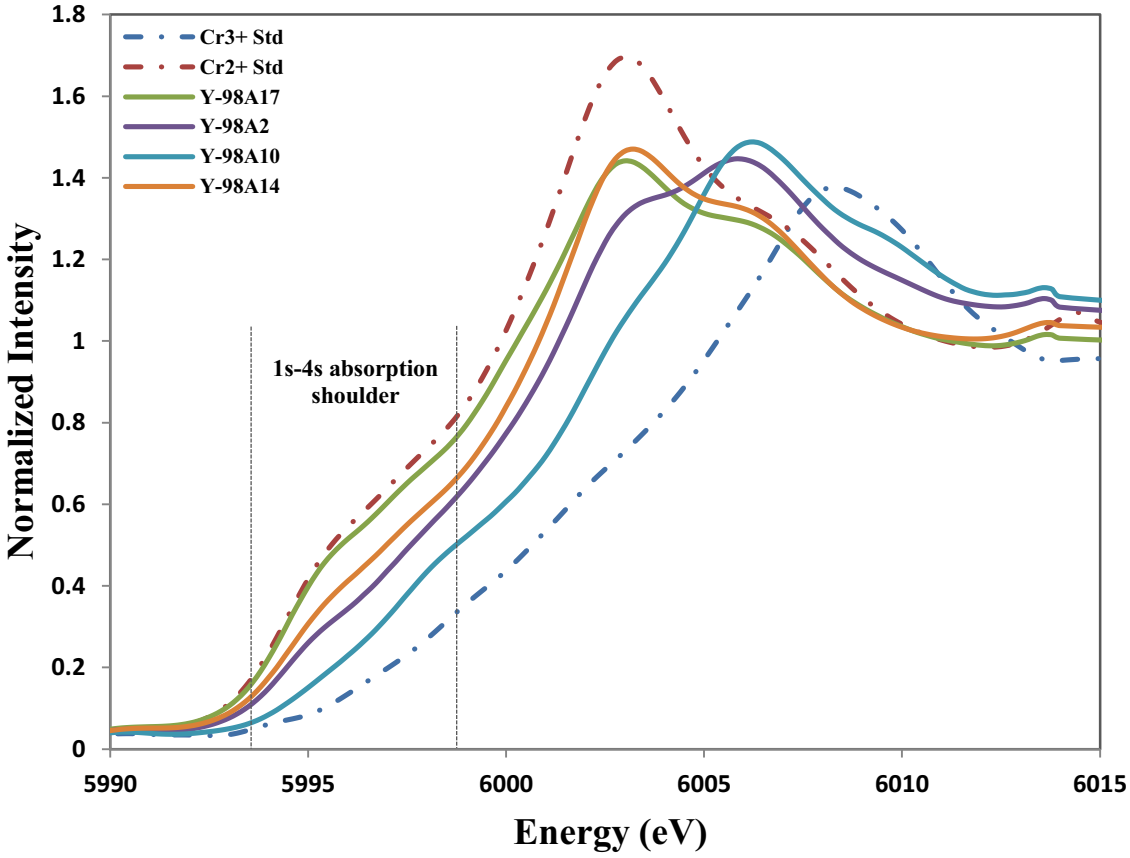

Figure 1 presents a few examples of normalized Cr K-edge spectra from Y-98A series olivine as well as the spectra from the Cr^{3+} and Cr^{2+} standard materials. Note the increasing intensity of the 1s-4s feature as the abundance of Cr^{2+} is increased relative to Cr^{3+}.

Figure 2

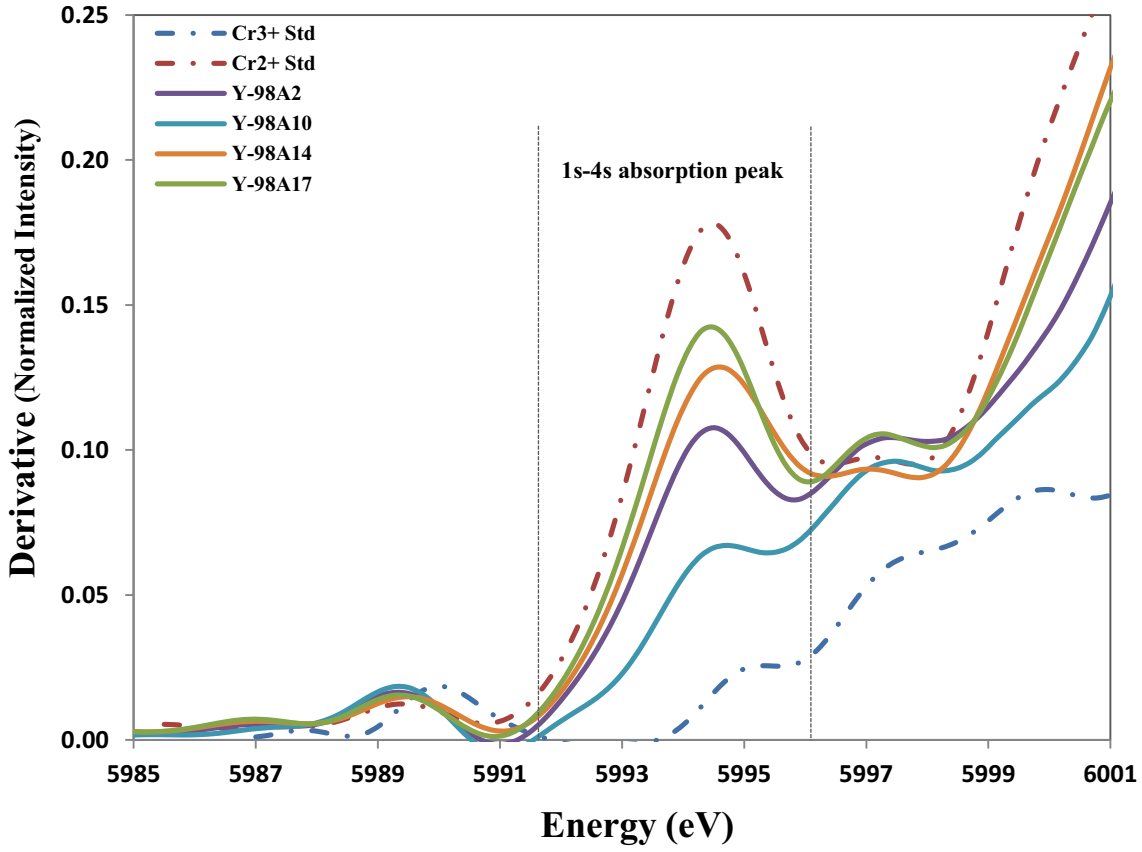

Figure 2 presents the derivatives of the same spectra that were plotted in Fig. 1. The 1s-4s absorption features show a clear, systematic change in intensity that scales with the Cr^{2+}/Cr^{3+} ratio.

Figure 3a & 3b

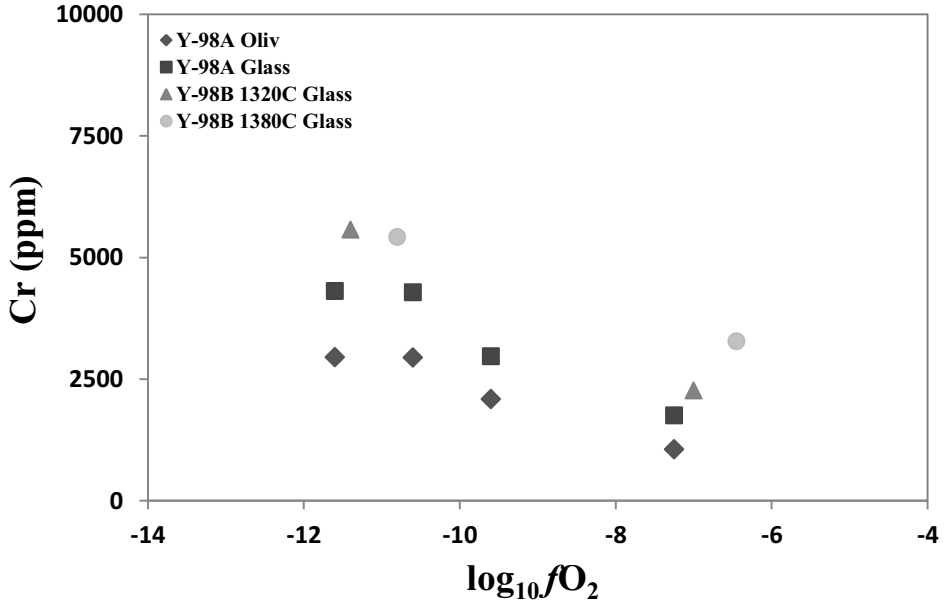

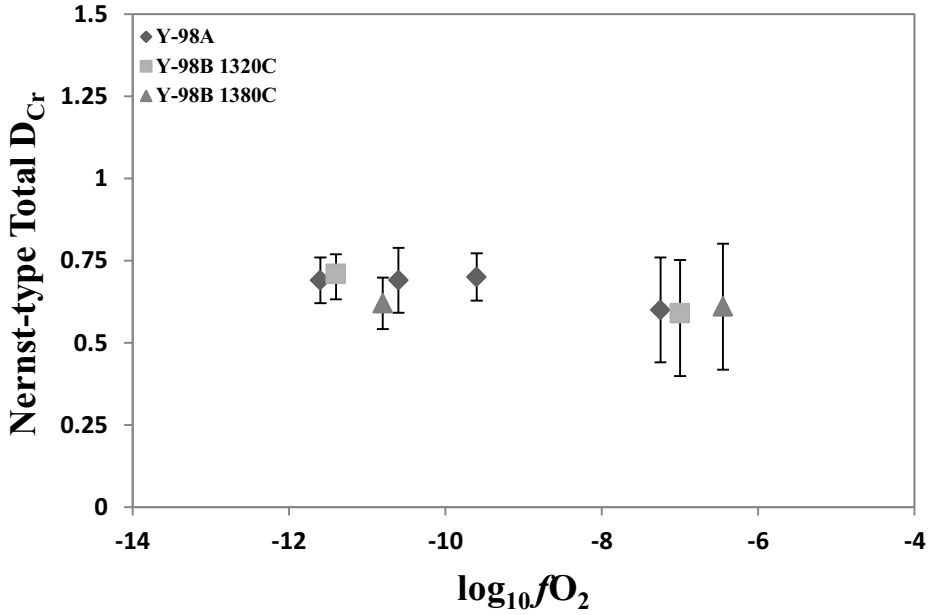

Figure 3a shows how the Cr content of both the melt and its equilibrium olivine decrease as a function of fO_2. The stabilization of Cr as the liquidus phase in the more oxidized experiments is responsible for this decrease. Figure 3b is a plot of the total Cr partition coefficient as a function of fO_2.

Figure 4

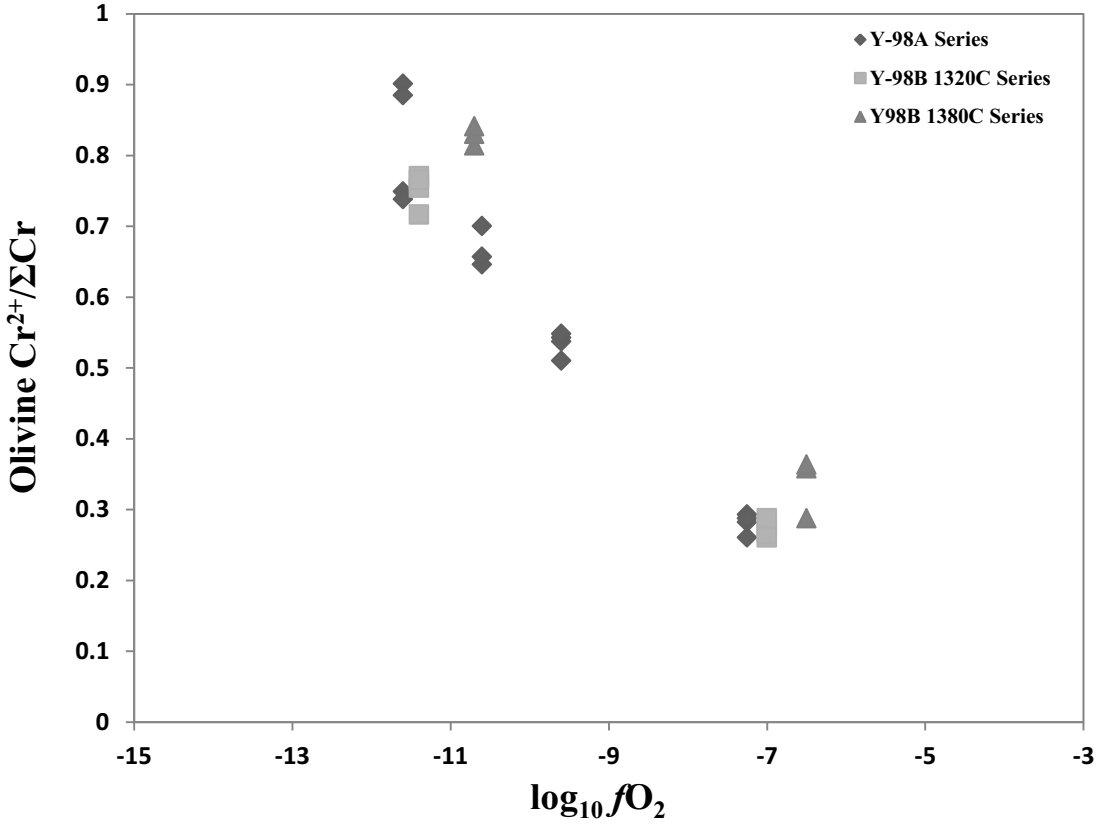

Figure 4 is a plot of the XANES determined $Cr^{2+}/\Sigma Cr$ vs. $\log_{10} fO_2$ for experimental olivine crystals from all of the experimental charges. We also point out the striking similarity between the values for the Y-98A series and the Y-98B 1320˚C series.

Figure 5

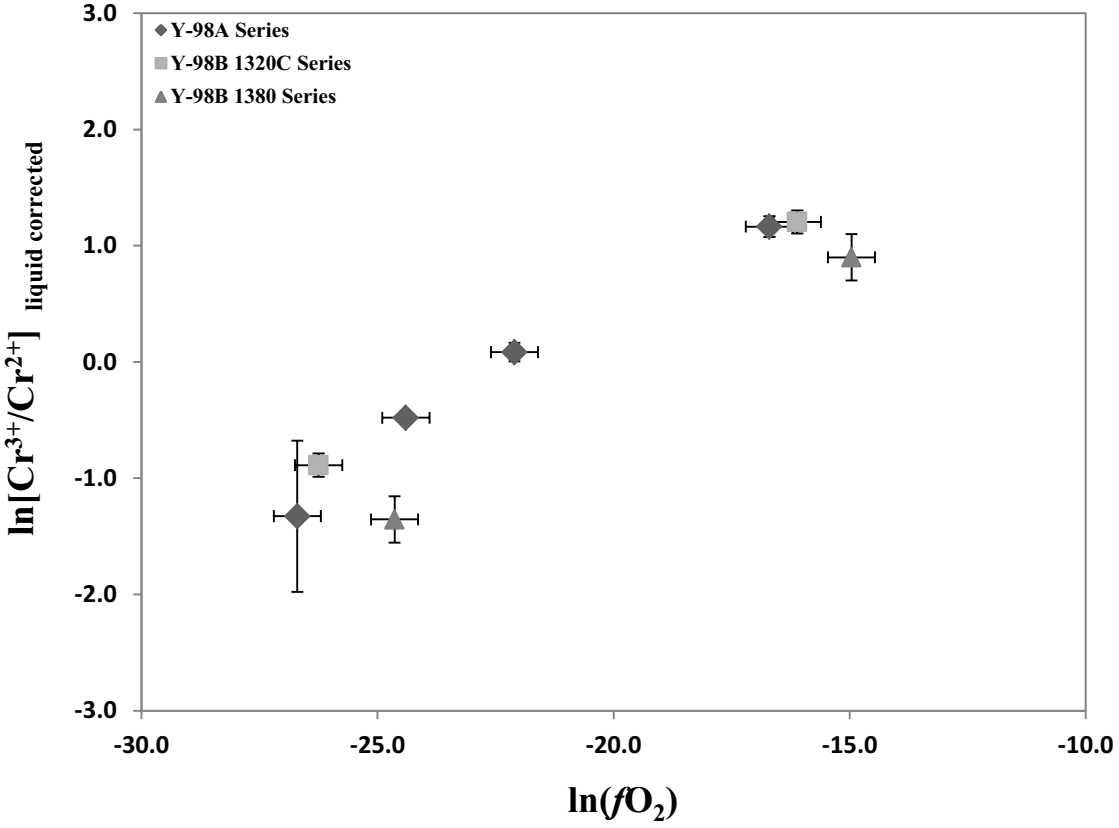

Figure 5 is a ln-ln plot of the average molar ratio of divalent to trivalent Cr in the liquid vs. fO_2. The plotted Cr^{3+}/Cr^{2+} values were corrected from the measured olivine values to those of the liquid. The regression slope for the Y-98A experiments is 0.24 with an R^2=0.97. This slope is in excellent agreement with the slope of 0.25 that is dictated by the stoichiometry of the homogenous Cr redox equilibrium.

Figure 6

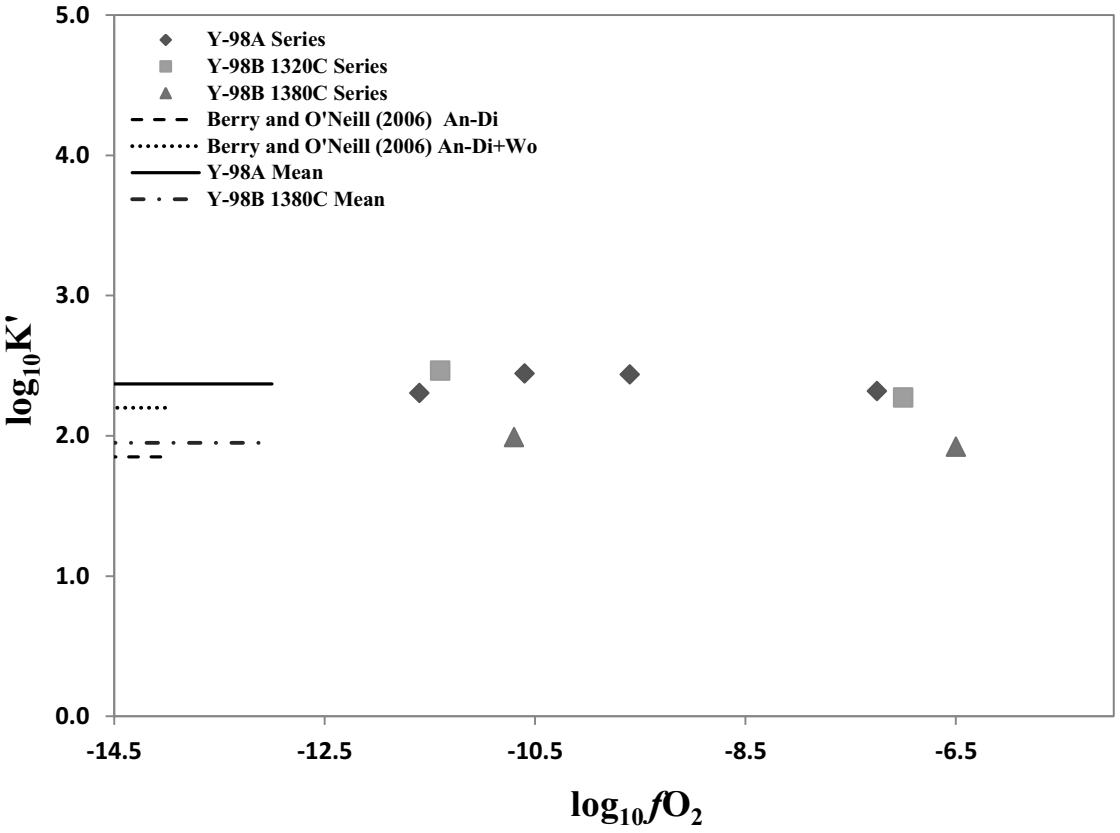

Figure 6 displays the logarithm of the apparent equilibrium constants plotted vs. logfO_2. The dashed lines represent mean logK' values from this study as well as logK' values derived from Berry and O'Neill (2006) for comparison. Note that the Berry and O'Neill (2006) data was obtained for Fe-free analog basalts at 1400˚C. The fO_2 invariance of the data is affirms the assumption that Cr obeys Henry's law in the Y-98 m

Figure 7

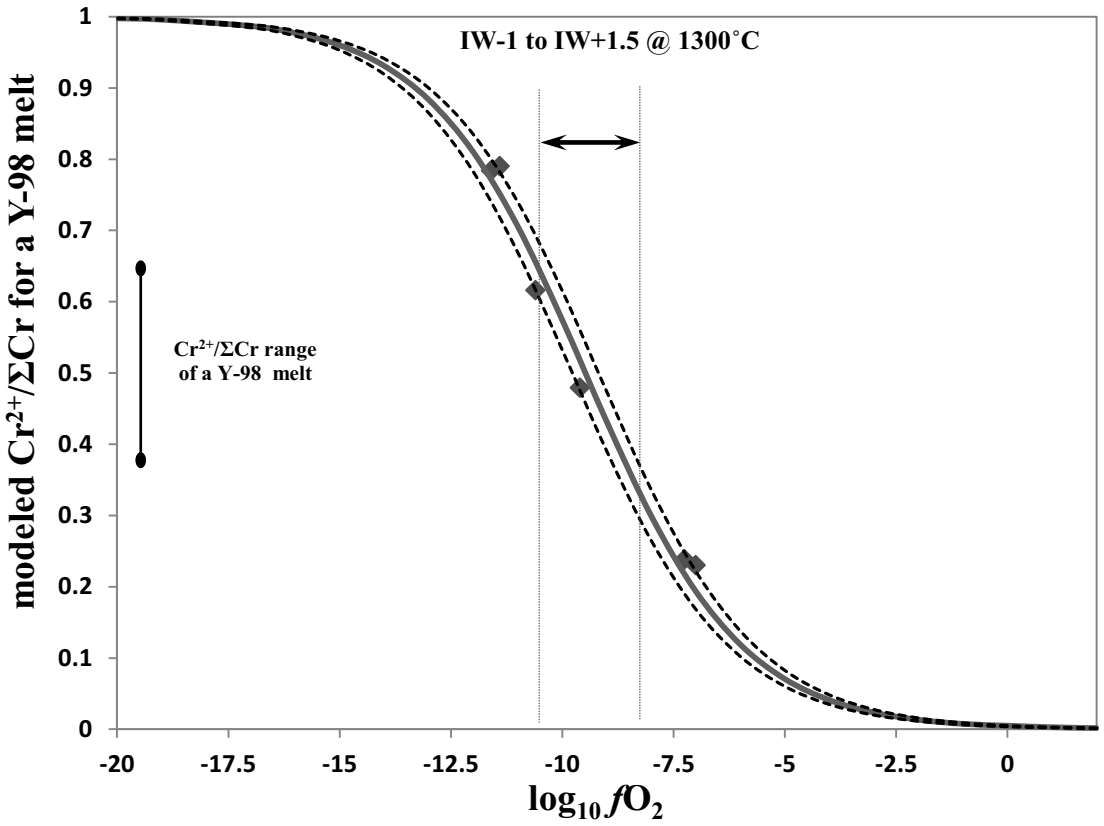

Figure 7 shows the $Cr^{2+}/\Sigma Cr$ modeled with the logK' values determined in this study. The points plotted along with the curve are the mean $Cr^{2+}/\Sigma Cr$ values from the Y-98A and Y-98B (1320˚C) experiments from which the apparent equilibrium constants used in the construction of the curve were derived. The dashed lines represent the 1σ uncertainty associated with the calculated curve (based on the 1σ standard deviation of the calculated logK' values). The arrows and dashed lines in the plot represent the range of fO_2 values that are thought to be representative for many primitive martian magmas.

Figure 8

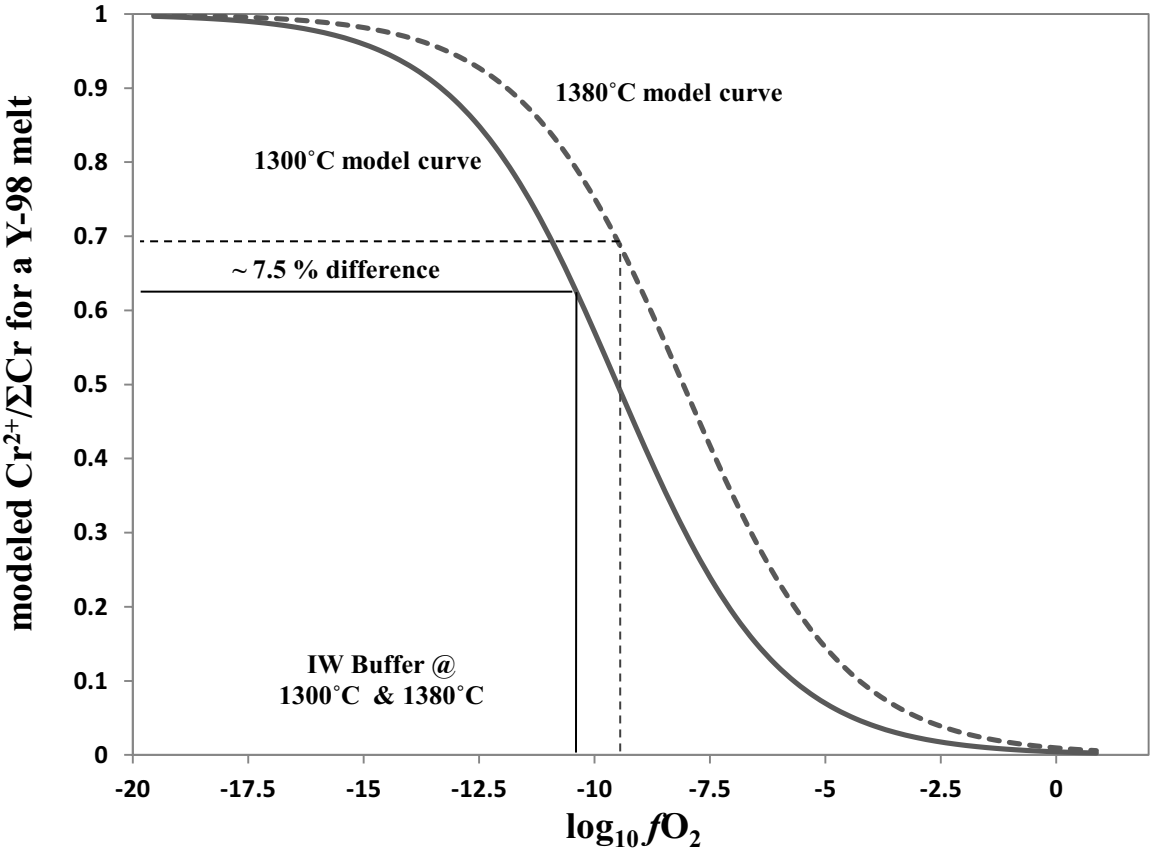

Figure 7 shows the $Cr^{2+}/\Sigma Cr$ modeled with the logK' values determined in this study. The points plotted along with the curve are the mean $Cr^{2+}/\Sigma Cr$ values from the Y-98A and Y-98B (1380˚C) experiments from which the apparent equilibrium constants used in the construction of the curve were derived. Notice how the Cr redox curve is displaced to higher fO_2 values as temperature is increased. The solid line represents the location of the IW buffer at 1300˚C and the dashed line represents the location of the buffer at 1380˚C. Simply increasing the temperature at a constant relative fO_2 value imparts an 8.5% increase in the Cr/ΣCr of the melt.